

NUMERICAL EXPLORATION OF A HEXAGONAL STRING BILLIARD

HANS L. FETTER

ABSTRACT. In this paper we are interested in the motion of a ball inside a billiard table bounded by a particular smooth curve. This table belongs to a family of billiards which can all be drawn by a common process: the so-called gardener's string construction. The classical elliptical billiard is, of course, the foremost member of this family. So it should come as no surprise that our hexagonal string billiard shares many basic properties with the latter, but, on the other hand, also exhibits some essential differences with it.

1. BACKGROUND

Let us consider the motion of a point inside a plane billiard table bounded by a closed convex curve. This point will always move along a straight line until it hits the boundary where it is reflected according to the well known principle: the angle of reflection is equal to the angle of incidence.

In order to get a billiard table with a sufficiently smooth boundary we can use the familiar method known as the gardener's or the string construction. First we need to choose some convex polygon K and then we proceed to wrap a loop of inelastic string around it, pulling the string tight at a point P and then moving this point P around. Note that when this technique is applied to a closed line segment one obtains an ellipse. Much is known about the billiard problem inside an ellipse: see for instance the books by Chernov and Markarian[6] and Tabachnikov[35], and also the articles by Berry[4], Korsch and Zimmer[21] and Acquistapace[1] just to name a few.

Another choice for the convex polygon which has received a fair amount of attention is that when K is an equilateral triangle. References include Hubacher [18], Gutkin and Katok [13], Gutkin and Knill[14], Turner [36]. Here again the result is a convex domain whose boundary is comprised of portions of ellipses.

In Fig. 1 we illustrate the gardener's construction of a table Ω for the case when K is a regular hexagon. The point P , as it moves around, traces out a curve $\partial\Omega$ which again consists of a certain number of elliptical arcs.

Varying the length l of the inelastic string one gets, of course, a whole family of billiard tables. We need to restrict our attention, however, to only one special value of l . This choice is dictated by the smoothness we get for the boundary $\partial\Omega$. So it is for it only for this particular case that we want to obtain a description, as complete as possible, of all the trajectories as the billiard ball (point particle) bounces elastically off the walls.

In closing this introduction let us just mention that the study of billiards and in particular the subject of billiards inside smooth convex curves is a very active area of research in the field of dynamical systems. The interested reader may consult

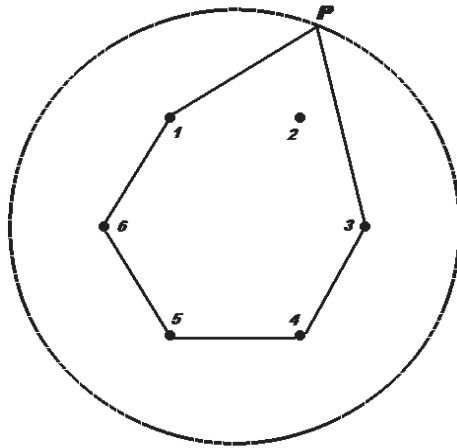


FIGURE 1. Hexagonal string billiard

some of the following books and research articles dealing with various important aspects of this topic (see [20, 22, 6, 35] and [2, 13, 14, 15, 18, 23, 26] respectively).

2. A FAMILY OF BILLIARDS OF CLASS C^2

The billiard table obtained by the string construction for an equilateral triangle, regardless of the string length used, is of class C^1 (see Hubacher [18]). In general, this is also true for all the other billiard tables obtained from regular polygons by the string construction, including the regular hexagon. However, with a proper choice of the string length l one can construct a table having greater regularity. To accomplish this let us first outline the setup and also the strategy behind the construction process for a whole family of “smooth” string billiards. To start we select K as any convex regular n -gon ($n \geq 5$). So right from the beginning we exclude both the equilateral triangle and the square from further considerations. The reason for that is because we need to be able to stellate K . A stellated polygon can be derived from a regular polygon by adding identical (congruent) isosceles triangles to all its sides. Instead of adding them all we add only one of those triangles to our given polygon K . The perimeter of this resulting polygon is the sought for special value for the string length l . Shortly we shall find an explicit expression for it. A portion of a regular polygon having vertices F_1, F_2, \dots, F_n with side length 2 is shown in left part of Fig. 2. The coordinates of the vertices, in terms of the interior angle $\alpha = \frac{n-2}{n}\pi$, are as indicated below:

$$\begin{aligned}
 F_1 &= [-1, 0] \\
 F_2 &= [1, 0] \\
 F_3 &= [1 - 2 \cos \alpha, -2 \sin \alpha] \\
 F_4 &= [-1 - 2 \cos \alpha + 4 \cos^2 \alpha, 2(-1 + 2 \cos \alpha) \sin \alpha] \\
 &\dots \\
 F_{n-1} &= [1 + 2 \cos \alpha - 4 \cos^2 \alpha, 2(-1 + 2 \cos \alpha) \sin \alpha] \\
 F_n &= [-1 + 2 \cos \alpha, -2 \sin \alpha]
 \end{aligned}$$

Now let us add the isosceles triangle with top vertex G_1 to the side F_1, F_2 (see left part of Fig. 2). In this figure we have actually added several identical (congruent) isosceles triangles to the sides of the regular n -gon. They have vertices G_1, G_2, \dots, G_n , whose coordinates are given below:

$$\begin{aligned}
 G_1 &= \left[0, -\frac{\sin \alpha}{\cos \alpha} \right] \\
 G_2 &= \left[\frac{\cos \alpha - 1}{\cos \alpha}, 0 \right] \\
 &\dots \\
 G_n &= \left[-\frac{\cos \alpha - 1}{\cos \alpha}, 0 \right]
 \end{aligned}$$

Each of the equal sides of the isosceles triangle $F_1 F_2 G_1$ has length $d = |F_1 G_1| = |F_2 G_1| = -1/\cos \alpha$.

So finally we get the expression for the particular string length we were looking for:

$$l = 2(n - 1) + 2d = 2(n - 1) - \frac{2}{\cos(\frac{n-2}{n}\pi)}$$

So much for the setup. In the right part of Fig. 2 we illustrate the result of the construction process described above for the case when K is a regular nine-gon. That we get billiard tables with greater regularity than just C^1 is the contents of the following theorem.

Theorem 2.1. *The generalized gardener's construction with length of the string*

$$l = 2(n - 1) - \frac{2}{\cos(\frac{n-2}{n}\pi)}$$

provides us with a family of billiard tables (one for each convex regular n -gon, $n \geq 5$) which are globally C^2 .

For the proof see A.

Some immediate consequences from this construction process include the following:

- As opposed to the general case we need to concern ourselves with only one kind of ellipse.
- The closed boundary curve we get is a smooth union of n elliptical arcs. In the general case one gets twice that number.

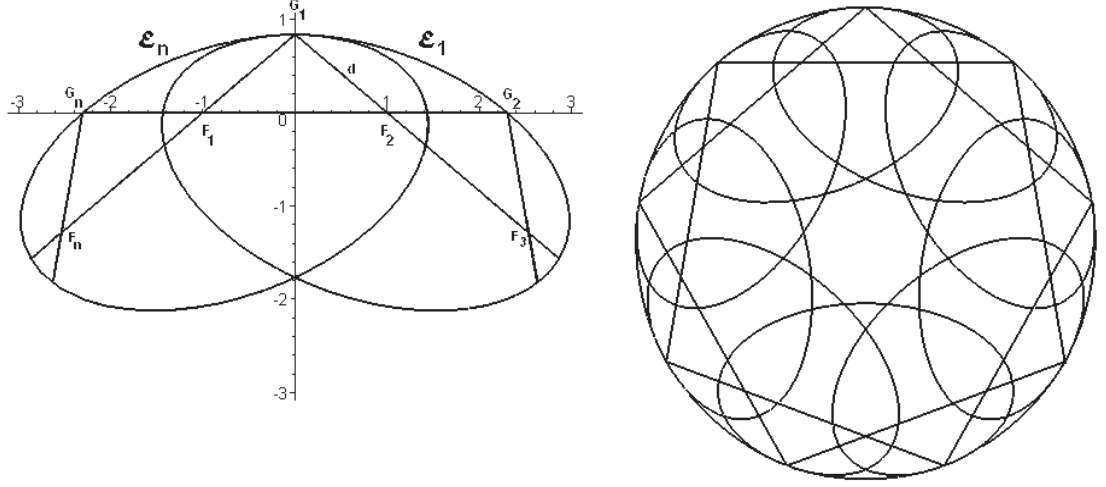


FIGURE 2. Construction of n -gonal string billiard and enneagonal string billiard

- Since an ellipse will always have strictly positive curvature the curvature κ is a continuous, strictly positive function on $\partial\Omega$.

From this point on we shall discuss one specific billiard only: the hexagonal string billiard. We shall now provide some specific details for it (see Fig. 3). Let K be the regular hexagon with sidelength 2. Its vertices have the coordinates

$$\begin{aligned} F_1 &= (-1, \sqrt{3}), & F_2 &= (1, \sqrt{3}), & F_3 &= (2, 0) \\ F_4 &= (1, -\sqrt{3}), & F_5 &= (-1, -\sqrt{3}), & F_6 &= (-2, 0) \end{aligned}$$

Since $n = 6$, $\alpha = \frac{2\pi}{3}$ and $d = -1/\cos\alpha = 2$ the length of the string $l = 2(n-1) + 2d = 14$. Each of the six elliptical arcs uses a unique pair of foci F_i, F_j , where i and j are either both even or both odd. To reflect this in our notation, we have used arc \widehat{ij} for an arc focused at F_i, F_j .

The equation for the arc $\widehat{24}$ is

$$\frac{(x-1)^2}{6} + \frac{y^2}{9} = 1$$

whereas the equation for the arc $\widehat{13}$ is given by

$$11y^2 + 2\sqrt{3}(x-6)y + 9x^2 - 12x = 60$$

At the common point $(3, \sqrt{3})$ the first derivative for both yields $-\sqrt{3}$ while the second derivative is $-\frac{3}{2}\sqrt{3}$.

As for the curvature κ of any elliptical arc, a simple calculation gives:

$$\frac{\sqrt{6}}{9} \leq \kappa \leq \frac{3\sqrt{3}}{16}$$

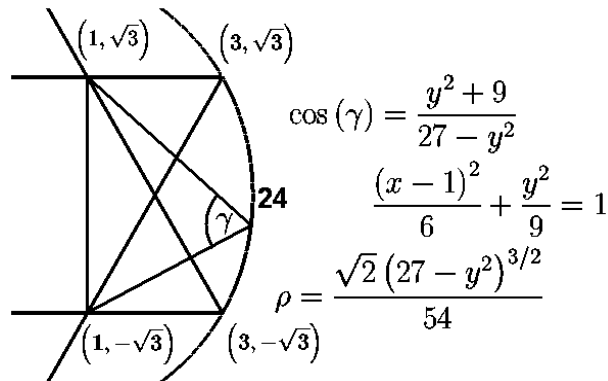


FIGURE 3. Data of hexagonal billiard

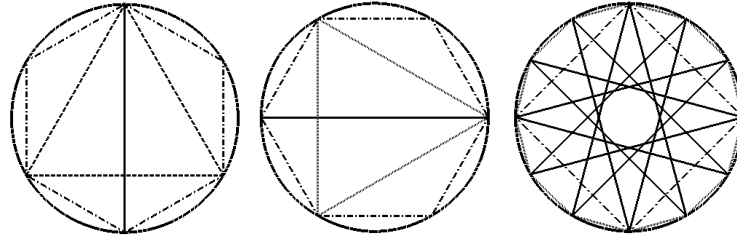
3. TYPES OF ORBITS

The orbits of billiards are sequences of line segments on the billiard table with the segments corresponding to the straight paths which the ball must follow within the region until it hits the boundary where it reflects elastically. Each such orbit is determined by the choice of the initial location for the billiard ball as well as the direction for the shot.

It is well-known that in a generic or typical billiard one can identify different types of trajectories: periodic, quasi-periodic (librational), whispering-gallery (rotational) and chaotic. We shall try to describe and illustrate them in the context of the hexagonal string billiard.

3.1. Periodic orbits. In almost any study on billiards initial interest centers on periodic orbits: those in which the particle follows the same path endlessly. In general these paths can be recognized easily because they simply correspond to inscribed simple polygons or star polygons. When, for example, a convex billiard table has two perpendicular symmetry axes then we immediately get a period four orbit (Hasselblatt and Katok [16]). Our billiard has six axes of symmetry, so we get twelve points from their intersection with the boundary of the billiard table. Selecting arbitrarily any of these points as the initial point and then connecting it to the next one by skipping over exactly $k - 1 = 0, \dots, 5$ intermediate points we are bound to get a closed figure. Since this figure is always invariant under the symmetries, it follows that at each point of intersection with the table the angle of incidence is equal to the angle of reflection. Now, according as $k = 1, \dots, 6$ the corresponding periodic orbits will close onto themselves after $\frac{12}{(12,k)}$ bounces, respectively, where (n, k) denotes the greatest common divisor of n and k . Some of these basic periodic orbits for our billiard are shown in Fig. 4.

When dealing with periodic trajectories a very natural question is: how many are there performing n bounces and at the same time going around the boundary k times? Birkhoff [5] provided an astonishing answer to the previous question as early as 1927 (see also Tabachnikov [35]):



(a) Unstable orbits of period 2, 3, and 6 (b) Stable orbits of period 2, 3, and 6 (c) Unstable orbits of period 4, 12, and 12

FIGURE 4. Periodic orbits $\left\{ \begin{smallmatrix} 12 \\ k \end{smallmatrix} \right\}$ where $k = 1 \dots 6$

Theorem 3.1. *For any $n \geq 2$ and every $k < \frac{n}{2}$, relatively prime, there exist two geometrically distinct n -periodic trajectories with the rotation number k .*

So, for example, the 2-,3- and 6-bounce orbits in Fig. 4(a) and those in Fig. 4(b) are geometrically distinct. They are similar though, with a similarity ratio of

$$\frac{2\sqrt{3}(-1 + \sqrt{6})}{5} = 1.0042$$

From Birkhoff's theorem we are lead to the conclusion that there are always at least $\varphi(n)$ distinct n -periodic trajectories, where $\varphi(n)$ denotes Euler's totient function. Thus when $n = 17$ we must have $\varphi(17) = 16$ distinct 17-periodic trajectories. The reader can appreciate the eight unstable 17-sided star polygons that we constructed for the hexagonal string billiard in Fig. 5.

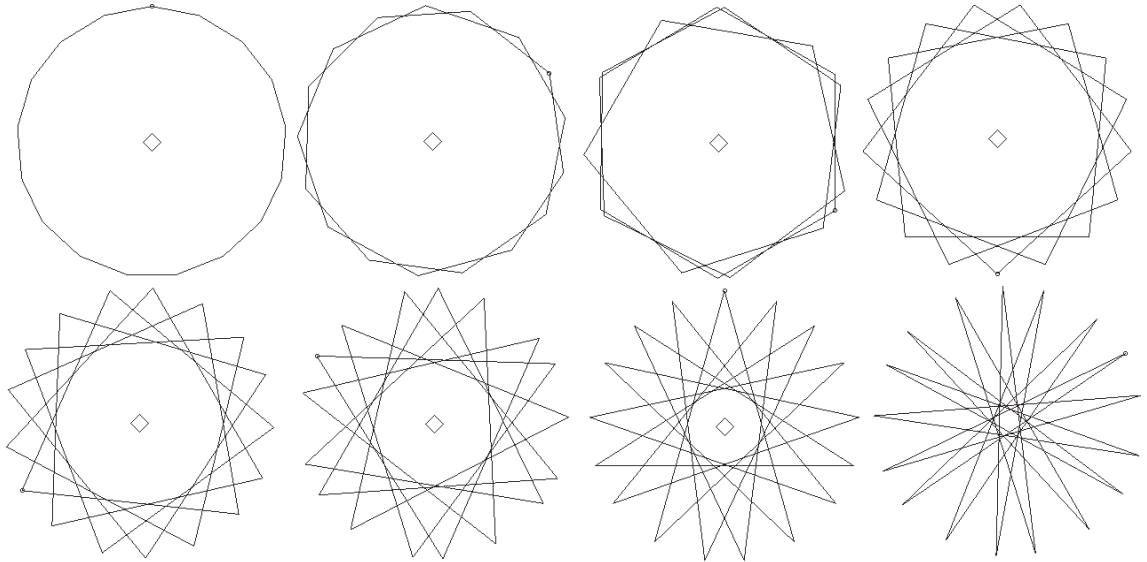


FIGURE 5. Star polygons: $\left\{ \begin{smallmatrix} 17 \\ 1 \end{smallmatrix} \right\} \dots \left\{ \begin{smallmatrix} 17 \\ 8 \end{smallmatrix} \right\}$

It is clear that, because our billiard has six-fold symmetry, we can rotate these geometrically distinct n -periodic trajectories by certain angles. The order of rotational symmetry is given by $\frac{6}{(6,n)}$ and so this yields a grand total of

$$\frac{6}{(6,n)}\varphi(n)$$

n -periodic trajectories for each $n \geq 3$.

The first few values of this expression are given in the following Table 1.

n	$\frac{6}{(6,n)}\varphi(n)$	n	$\frac{6}{(6,n)}\varphi(n)$
3	4	8	12
4	6	9	12
5	24	10	12
6	2	11	60
7	36	12	4

TABLE 1. Total number of n -gons.

3.2. Quasi-periodic orbits. Sometimes one also encounters certain orbits which explore only restricted parts (segments) of the boundary $\partial\Omega$. Every (stable) simple polygon or star polygon (the two-bounce orbit included) gives rise to an infinite number of these quasi-periodic orbits. They resemble the underlying polygons: it is as if these just fattened up. So that's why we will also refer to them simply as fat (star) polygons. Orbits which explore 2, 3, 4, 6 and 9 parts can be seen in Figs. 6 and 7. More examples can be found in Figs. 10, 14, 22 and 24.

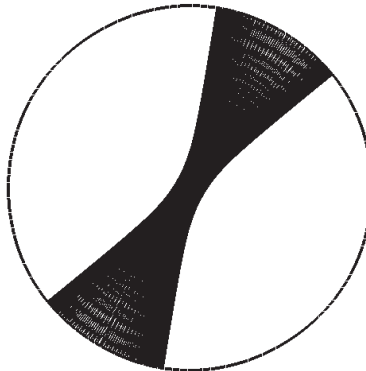


FIGURE 6. A typical bouncing orbit or fat polygon of type $\left\{ \begin{smallmatrix} 2 \\ 1 \end{smallmatrix} \right\}$

3.3. Whispering gallery orbit. Another kind of orbits, which on occasions are also referred to as *skipping* trajectories (see Berry [4], Chernov and Markarian[6]), are very common for most billiards. They are characterized by the fact that they bounce all round $\partial\Omega$ densely filling a ring-like shaped region.

There are many of these orbits in our billiard and we show several of them in Fig. 8.

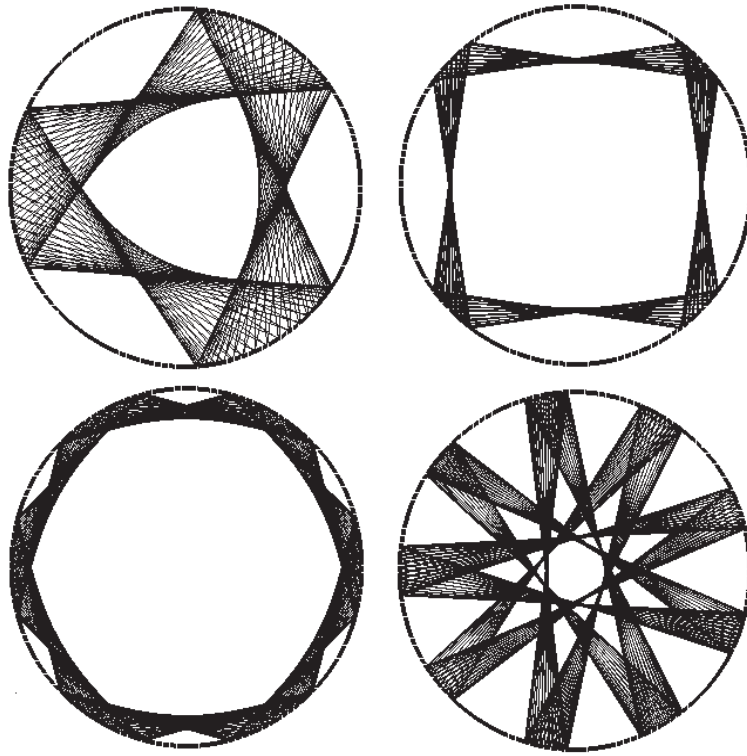


FIGURE 7. Quasi-periodic orbits or fat polygons of type: $\begin{Bmatrix} 3 \\ 1 \end{Bmatrix}$, $\begin{Bmatrix} 4 \\ 1 \end{Bmatrix}$, $\begin{Bmatrix} 6 \\ 1 \end{Bmatrix}$ and $\begin{Bmatrix} 9 \\ 4 \end{Bmatrix}$

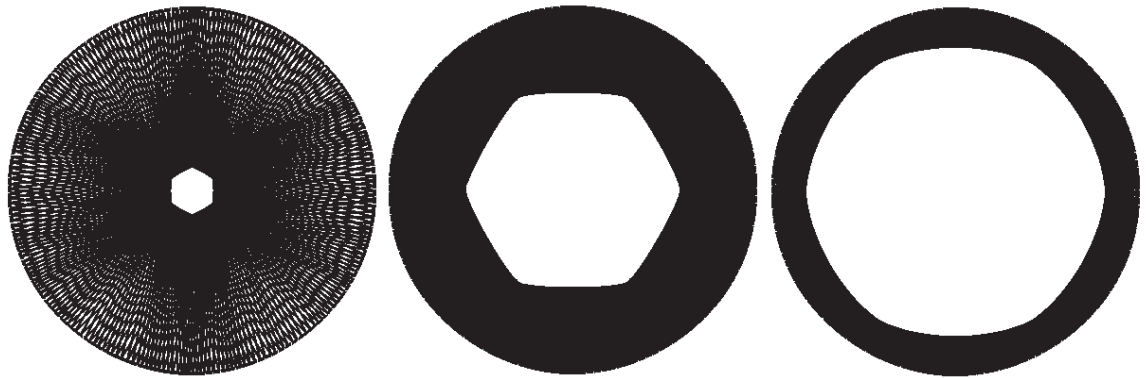


FIGURE 8. Whispering gallery type orbits

3.4. Chaotic orbit. Most billiards exhibit chaotic behavior to some extent (circles and ellipses excluded). Chaotic trajectories look disordered, erratic and there is no discernible pattern. They usually manifest themselves more clearly in the surface of section, which we will introduce later. For the moment let us just say that there is no evidence that our billiard has these kinds of orbits.

4. SOME ANALOGOUS PROPERTIES OF THE ELLIPTICAL AND THE HEXAGONAL STRING BILLIARD

One of the most important properties of elliptic billiards is the following result which essentially tells us that we can group the trajectories into three families.

A trajectory for the billiard inside an ellipse either

- (1) always passes through the two foci alternately (focal trajectory), or
- (2) always intersects the open segment between the two foci (inner trajectory),
or
- (3) never intersects the closed segment between the foci (outer trajectory).

(See Siburg [32], Tabachnikov [35], Chernov and Markarian [6]).

In a completely analogous fashion for the hexagonal string billiard we also have three families of trajectories: focal, inner, and outer.

Theorem 4.1. *Consider a trajectory issuing from the point P_0 inside a hexagonal string billiard with vertices P_1, P_2, \dots .*

- i) *If the segment P_0P_1 of the billiard trajectory is on a supporting line of K , then every segment P_iP_{i+1} will be on a supporting line of K .*
- ii) *If the segment P_0P_1 of a billiard trajectory does intersect the hexagon K then all segments P_iP_{i+1} will intersect it.*
- iii) *If the segment P_0P_1 of a billiard trajectory does not intersect the hexagon K then no segment P_iP_{i+1} will intersect it.*

A sketch for the proof of this result can be found in B.

Another important result for the billiard inside an ellipse states that a billiard trajectory through the foci converges to the major axis of the ellipse. (See for example Tabachnikov [35], Batschelet [3], Frantz [10], Hasselblatt and Katok [16], Wilker [37], Moser and Zehnder [27]).

In practice this means that any focal orbit quickly becomes indistinguishable from a repeated tracing of the major axis of the ellipse.

Whereas a focal orbit in the case of the ellipse converges to the “to and fro” orbit (the unstable two-bounce orbit), in that of the hexagonal string billiard it converges to either one of the equilateral triangles (the unstable three-bounce orbits).

Before stating the result in more precise terms we need an auxiliary result which provides bounds for the sizes of the angles between incoming and outgoing rays in focal orbits. (See Fig. 3).

Theorem 4.2. *For a focal orbit of the hexagonal string billiard the angle between incoming and outgoing segments is limited to the range*

$$60^\circ \leq \gamma \leq 70.53^\circ$$

Proof in C.

Without loss of generality let us choose the three-bounce orbit shown in Fig. 4(a). The vertices for this triangle are $S_1 = (0, 2\sqrt{3})$, $S_3 = (3, -\sqrt{3})$, and $S_5 = (-3, -\sqrt{3})$. Consider a billiard trajectory, passing through the focus F_2 , whose initial point P_0 is on arc $\widehat{24}$. See Fig. 9. Observe that, for example, point P_4 is closer to point S_1 than P_1 , and then P_7 is even closer to it and so on. Already we find that $P_7P_8P_9$ resembles triangle $S_1S_5S_3$ very much.

Under these circumstances we have:

Theorem 4.3. *If a billiard trajectory travels along a supporting line of K , so that it goes alternately through the focal points F_2, F_6, F_4 then its trajectory will quickly become indistinguishable from a repeated tracing of the triangle $S_1S_5S_3$.*

See D for proof.

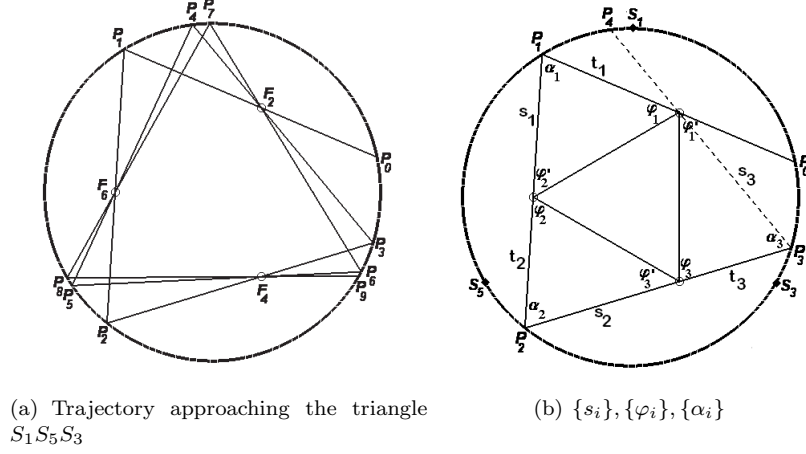


FIGURE 9. Focal orbits

5. STABILITY

Several authors include in their work a brief discussion on the stability of certain n -periodic orbits through the use of the so called deviation matrix M . We also want to mention something about stability. For this purpose we have chosen the $\begin{Bmatrix} 12 \\ 5 \end{Bmatrix}$ orbit, which can be seen on the top left part of Fig. 10. This orbit is not the same as the earlier one we came across in Fig. 4(c) (unstable $\begin{Bmatrix} 12 \\ 5 \end{Bmatrix}$ orbit).

So following Berry [4], Lopac et al. [25], [24], and Robnik [31] we have to construct the deviation matrix M corresponding to the selected orbit:

$$M = M_{1,2}M_{2,3} \cdots M_{12,1}$$

where each 2×2 matrix $M_{i,k}$ can be expressed as

$$M_{i,k} = \begin{pmatrix} -\frac{\sin \alpha_i}{\sin \alpha_k} + \frac{\rho_{ik}}{R_i \sin \alpha_k} & -\frac{\rho_{ik}}{\sin \alpha_i \sin \alpha_k} \\ -\frac{\rho_{ik}}{R_i R_k} + \frac{\sin \alpha_k}{R_i} + \frac{\sin \alpha_i}{R_k} & -\frac{\sin \alpha_k}{\sin \alpha_i} + \frac{\rho_{ik}}{R_k \sin \alpha_i} \end{pmatrix}.$$

The symbol R_i (R_k) denotes the radius of curvature at the point of impact P_i (P_k), α_i (α_k) the angle which the departing ray makes with the tangent on the billiard boundary at the point of impact P_i (P_k) and ρ_{ik} the length of the path between two consecutive impact points P_i and P_k .

For our particular choice we only get two kinds of these 2×2 matrices $M_{i,k}$ since only the path lengths change between impacts, all other data remaining constant.

In fact, if we define

$$\tau = \frac{3\sqrt{(4947 - 2328\sqrt{3})}}{97}$$

then we get

- (1) $R_i = R_k = \frac{\sqrt{2}}{54} \left(\frac{2160+216\sqrt{3}}{97} \right)^{3/2}$
- (2) $\alpha_i = \alpha_k = 5\pi/12$, so that $\sin(\alpha_i) = \sin(\alpha_k) = \frac{\sqrt{2}(1+\sqrt{3})}{4}$
- (3) the two values which alternate

$$\rho_{ik} = \sqrt{\left(\frac{43}{3}\tau^2 + 8\sqrt{3}\tau^2 + 8\tau + 6\sqrt{3}\tau + 3 \right)}$$

$$\rho_{ik} = \frac{8}{3}\tau + \frac{4\sqrt{3}}{3}\tau + 2$$

So

$$M_{1,2} = M_{3,4} = M_{5,6} = M_{7,8} = M_{9,10} = M_{11,12} = T$$

$$M_{2,3} = M_{4,5} = M_{6,7} = M_{8,9} = M_{10,11} = M_{12,1} = S$$

where

$$T = \begin{pmatrix} 0.9830565623814575557 & -7.1795378524870580504 \\ 0.00467993843741796985 & 0.9830565623814575557 \end{pmatrix}$$

and

$$S = \begin{pmatrix} 0.9700724323780286883 & -7.1325295852446540944 \\ 0.00826627849706319570 & 0.9700724323780286883 \end{pmatrix}$$

Therefore our deviation matrix M turns out to be

$$M = (TS)^6 = \begin{pmatrix} -.87488446006857883011 & -17.010433690097981202 \\ .015415741802173798979 & -.84327883276452294763 \end{pmatrix}$$

Orbital stability depends on the eigenvalues of M . In fact, if by $\text{tr}(M)$ we denote the trace of M then it is known that (Berry [4]) we have the following possibilities:

- (1) if $|\text{tr}(M)| < 2$ then the orbit is stable
- (2) if $|\text{tr}(M)| > 2$ then the orbit is unstable
- (3) if $|\text{tr}(M)| = 2$ then the orbit is neutrally stable.

For our case we simply get that

$$\text{tr}(M) = -1.7181632928331017777$$

which guarantees the stability of our chosen orbit. This analytically verified stability can also be observed numerically: see Fig. 10, where in addition to the $\left\{ \begin{smallmatrix} 12 \\ 5 \end{smallmatrix} \right\}$ polygon we show several quasi-periodic orbits.

6. FORBIDDEN INNER REGION

In many of the figures (see for example Figs. 7, 8, 10) we can discern a closed convex proper subset \mathcal{F} of Ω which lacks segments of the corresponding billiard trajectory. We shall call it a “*forbidden inner region*”, a term which we have borrowed from Korsch and Zimmer [21]. It is separated from the allowed region by a non differentiable piecewise smooth closed curve. By all of this we are, of course, reminded of the notion of a caustic. There are several different meanings of the word caustic in billiards. The one that seems the most appropriate for us is (see Gruber [12], Klee and Wagon [19], Turner [36]):

A convex caustic for a convex table Ω is a closed convex proper subset \mathcal{C} of Ω such that whenever the initial segment of a billiard path in Ω lies in a supporting line of \mathcal{C} , then every later segment also lies in a supporting line of \mathcal{C} . All billiard tables obtained by the string construction have a special caustic. The hexagon K is such a caustic and we already established this in Theorem 4.1.

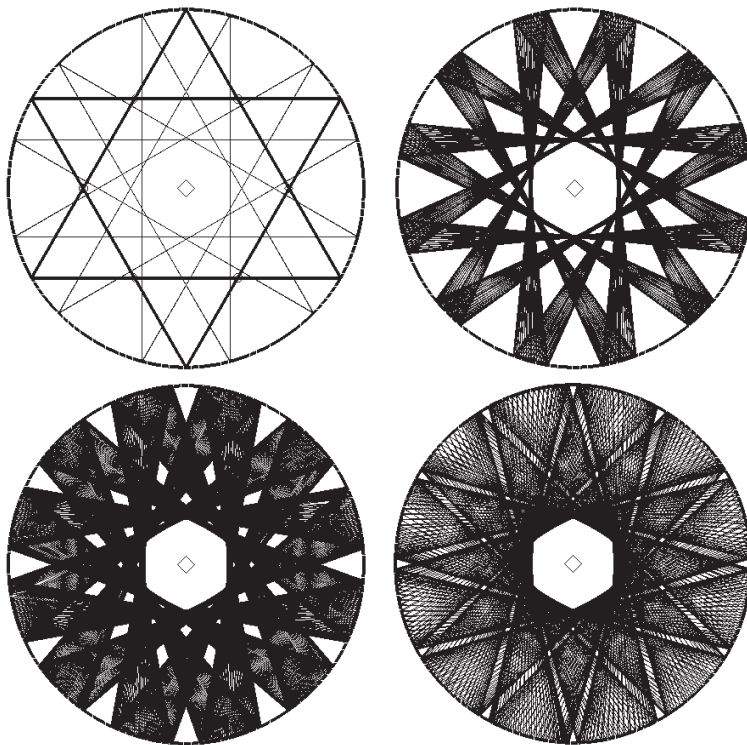


FIGURE 10. Stable $\left\{\begin{smallmatrix} 12 \\ 5 \end{smallmatrix}\right\}$ orbit and several fat $\left\{\begin{smallmatrix} 12 \\ 5 \end{smallmatrix}\right\}$'s

Are the forbidden inner regions we get in the other cases caustics as well? For us to have a convex caustic every line segment of a trajectory needs to touch \mathcal{C} . However careful inspection of the billiard trajectories reveals that a few line-segments do not touch \mathcal{C} (see Fig. 11).

We need to introduce an alternative description for the forbidden inner region. We define the forbidden inner region \mathcal{F} as the intersection of all the “left” half-planes to the lines containing the segments of a billiard trajectory (see Hasselblatt and Katok [16]).

We have included Fig. 11 which allows us to follow the construction process of a forbidden inner region with an increasing number of half-planes.

A problem remaining is that of trying to find an analytical expression for the piecewise smooth closed curve bounding the forbidden inner region. The orbits shown in Figs. 7, 8, 10 and 12 strongly suggest that a hexagon with curved sides might be appropriate for the curve we are looking for.

Using elliptical arcs for the sides of the curved hexagon we get the results shown in Fig. 13 and also in Fig. 14.

7. POINCARÉ SECTION

So far we have presented all orbits as merely sequences of directed line segments in the configuration space. This approach, even if we observe the evolution of a large number of these trajectories, gives us only a limited understanding of the

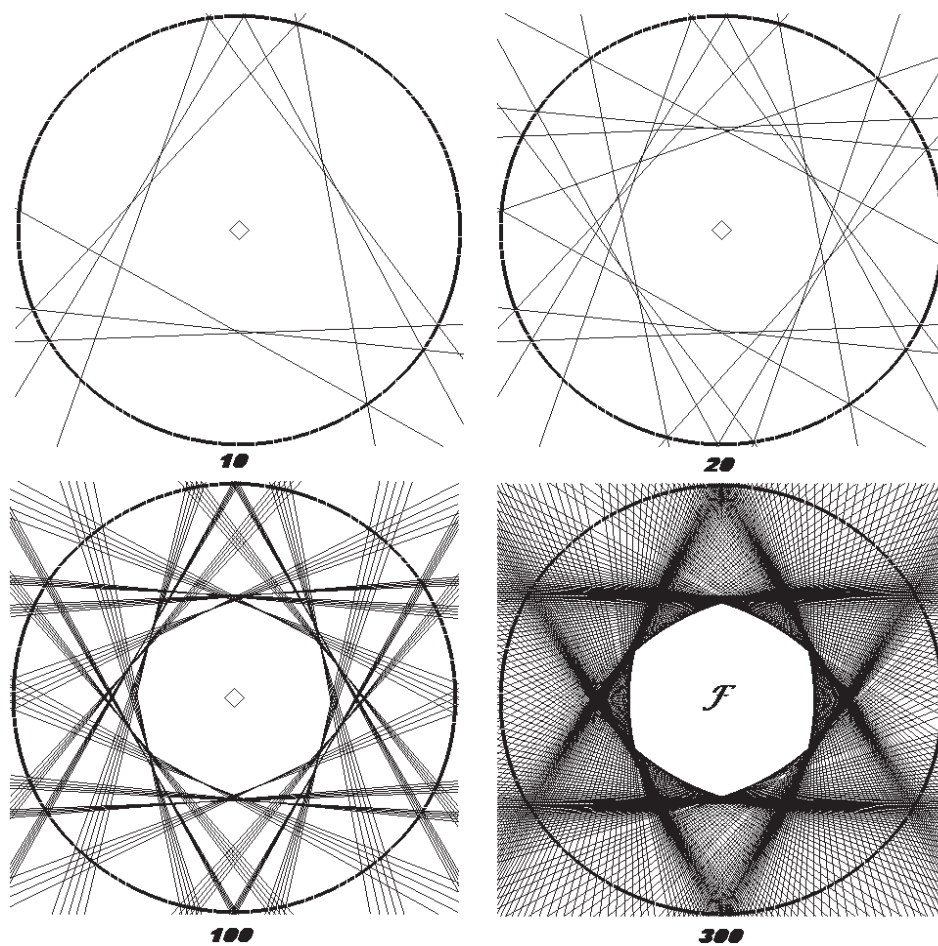


FIGURE 11. Construction of forbidden inner region

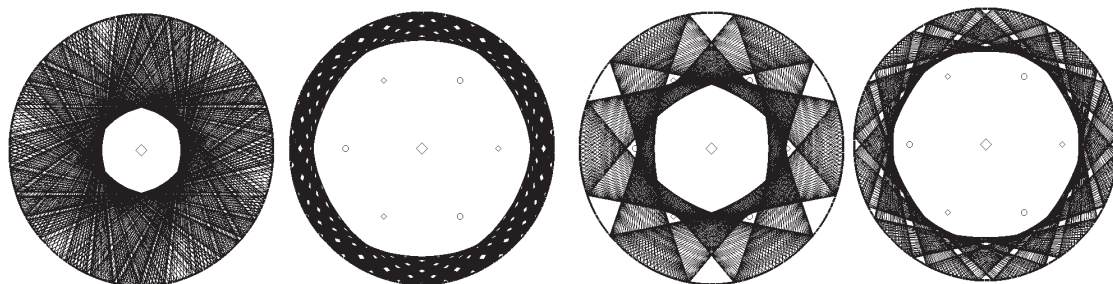


FIGURE 12. Forbidden inner regions for groups of quasi-periodic orbits:
 $6 \begin{Bmatrix} 5 \\ 2 \end{Bmatrix}' s$, $6 \begin{Bmatrix} 5 \\ 1 \end{Bmatrix}' s$, $2 \begin{Bmatrix} 3 \\ 1 \end{Bmatrix}' s$, and $3 \begin{Bmatrix} 4 \\ 1 \end{Bmatrix}' s$

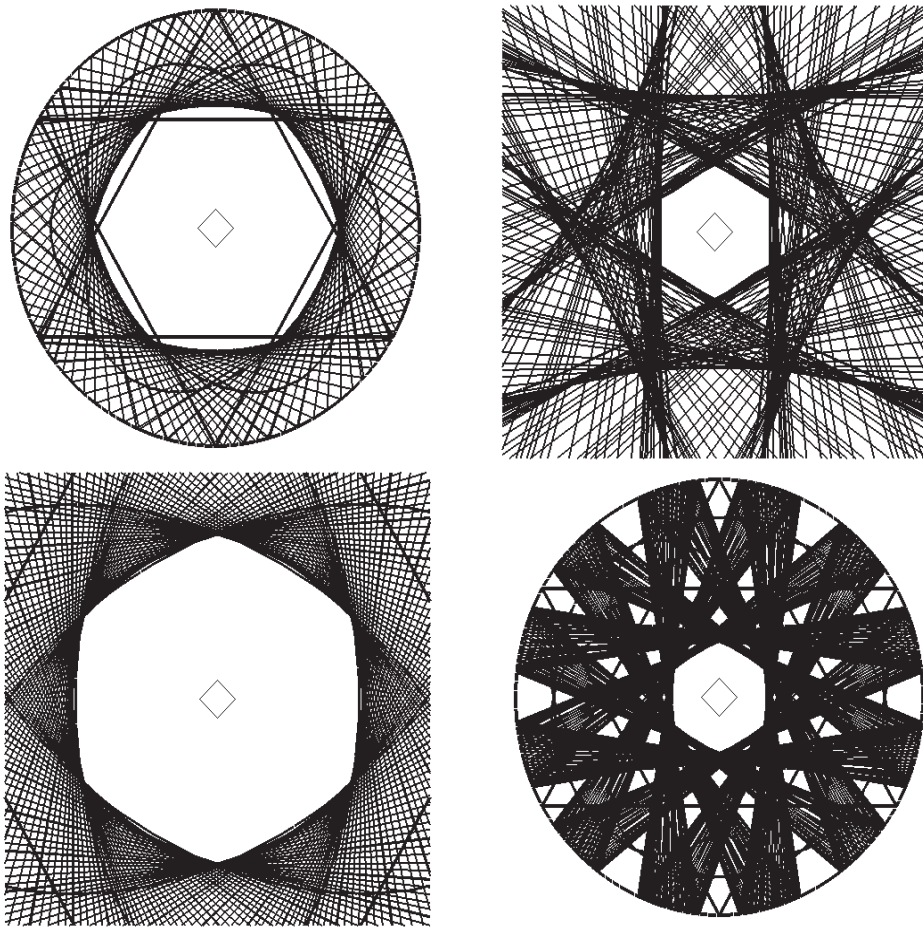


FIGURE 13. Arcs of ellipses separating forbidden inner region

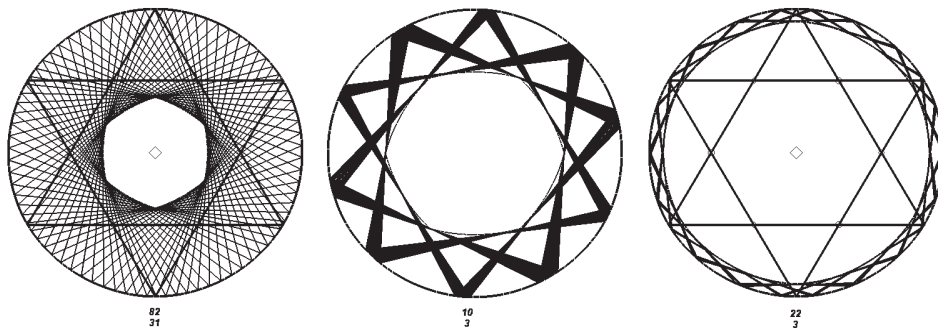


FIGURE 14. Piecewise smooth curve separating forbidden inner region

complicated dynamics associated with the motion. A more convenient way to visualize the dynamics is through the use of Poincaré's surface of section (SOS), which enables us to display the character of each particular trajectory. The surface of section, see for instance Sussman and Wisdom[34], can be described by means of two coordinates in the

- (1) horizontal direction: arc length s from an arbitrarily chosen fixed point O on the boundary of the billiard, and
- (2) vertical direction: the angle θ between positive tangent direction and outgoing or reflected billiard ray at a point of impact.

This then defines the following Poincaré section

$$\mathcal{P} := \{(s, \theta) | s \in [0, |\partial\Omega|], \theta \in [0, \pi]\}$$

There are, qualitatively speaking, three different classes of trajectories possible on a SOS, clearly differentiated by the dimension d of the subspace of the section that they explore (Berry[4], Hayli[17], Korsch and Jodl[20], Sussman and Wisdom[34]). They might

- (1) generate a finite set of k discrete points corresponding to a periodic orbit having period k ($d = 0$)
- (2) eventually fill out an invariant curve, which may either run from edge $s = 0$ to edge $s = 2\pi$ as an undulating line corresponding to a whispering-gallery or a focal orbit, or consist of a group of ovals or islands corresponding to a quasi-periodic orbit ($d = 1$)
- (3) scatter over a region eventually filling a whole area corresponding to an irregular or chaotic trajectory ($d = 2$).

Because our billiard has the same symmetry as a hexagon, we do not need to plot the entire surface of section. We shall usually only display the upper half of it and note the fact that the SOS is periodic with period six.

To give the reader an idea of the structure of the SOS we first present an image in which we have included points and curves corresponding to some 70 orbits, each followed through 480 bounces (see Fig. 15). In Fig. 16 we do not show all of them at once as was done before, but rather in small groups, for different ranges of the angle θ .

Several close-ups of the six-bounce orbits which can clearly be recognized in the plot on the right in the top row of Fig. 16 are shown in Fig. 17.

Another close-up (Fig. 18), this time of the bottom plot from Fig. 16 shows both undulating lines and ovals. The big ovals surround the invariant points corresponding to the stable periodic orbits associated with $\begin{Bmatrix} 12 \\ 5 \end{Bmatrix}$, $\begin{Bmatrix} 54 \\ 23 \end{Bmatrix}$, $\begin{Bmatrix} 7 \\ 3 \end{Bmatrix}$, and $\begin{Bmatrix} 30 \\ 13 \end{Bmatrix}$.

Finally, we decided also to include the curve generated in the surface of section by a large number of focal orbits (see Fig. 19). It is interesting to note that in this case it is even possible to get an explicit expression for each arc that appears. The coordinates of the points on a reference arc for the focal curve are given by

$$\left(E \left(\frac{\sqrt{(1 + 3 \cos(2y))(-1 + \cos(2y))}}{1 - \cos(2y)}, \frac{\sqrt{3}}{3} \right), y \right)$$

where

$$\frac{\arccos(-1/3)}{2} \leq y \leq \frac{\arccos(-1/2)}{2},$$

and $E(x, k)$ is simply an elliptic integral of the second kind (see Davis [7]).

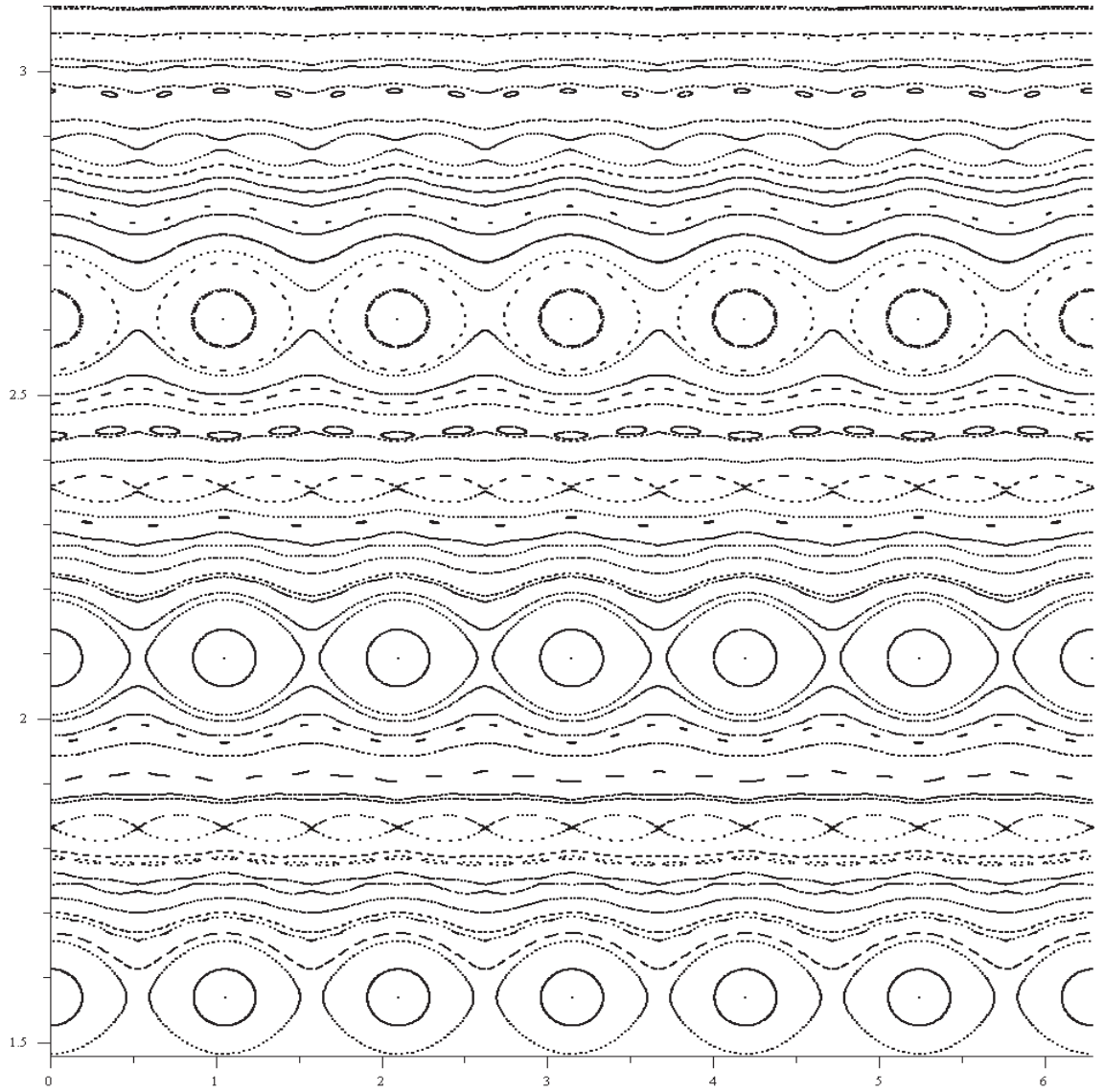


FIGURE 15. Surface of section: 70+ orbits followed through 480 bounces

8. ADDITIONAL PERIODIC ORBITS AND SOME COMMENTS ON THE STRUCTURE OF ORBITS IN CONFIGURATION SPACE

All the periodic orbits we have presented so far are those corresponding to star polygons of the kind $\{n/k\}$, with $1 \leq k < n/2$ and $(n, k) = 1$, which always come in pairs: one stable and the other one unstable. Moreover these orbits are isolated, as is customary for a generic billiard (Berry[4]).

So, now, a natural question arises as to whether there are any other periodic orbits besides those just mentioned. After all, many authors, among them Berry[4],

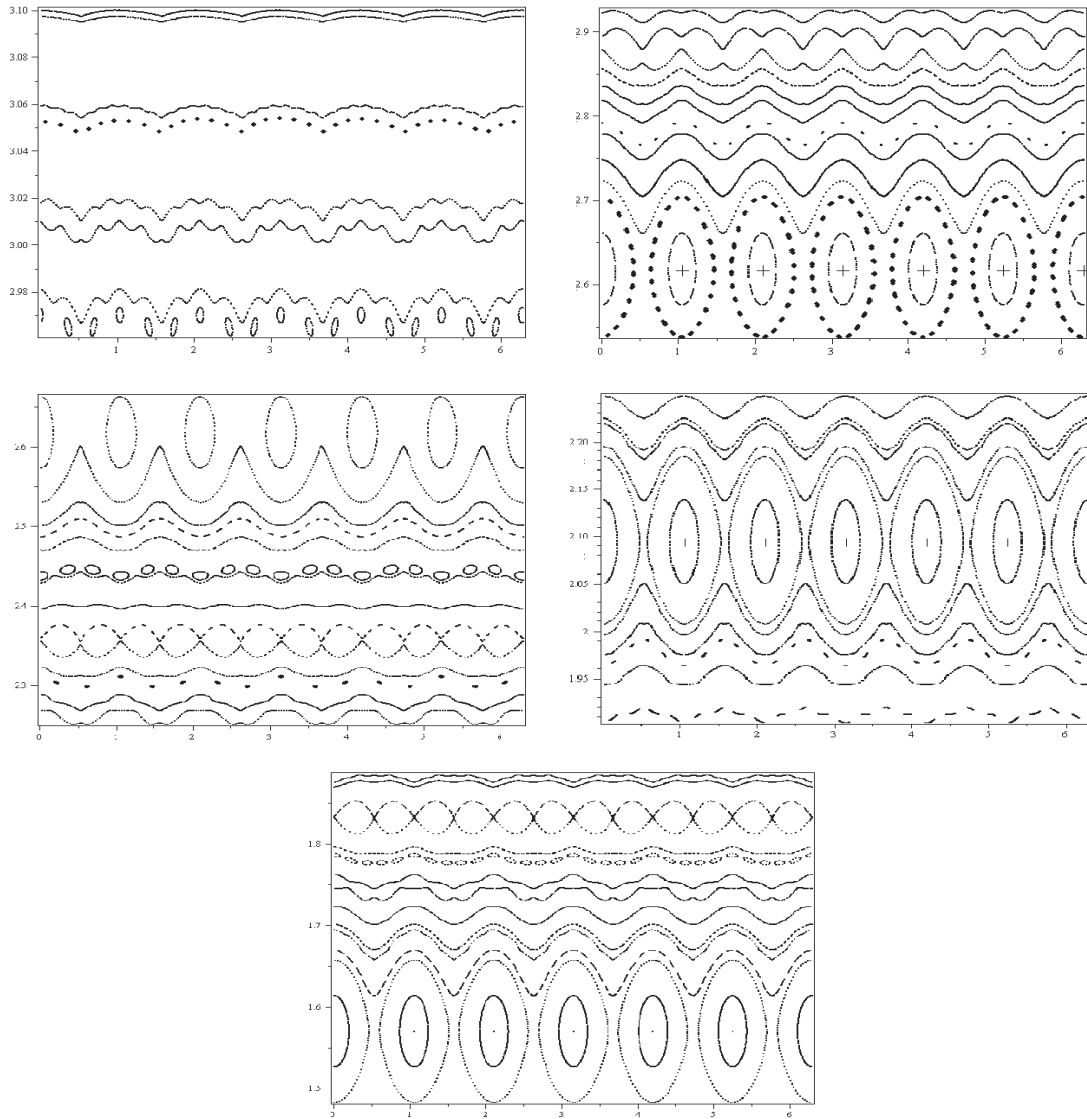


FIGURE 16. Surface of section: same as Fig. 15, but more detailed

Korsch and Zimmer[21], Okai et al.[28], and Sieber [33] include periodic orbits in their work which do not correspond to star polygons. Of course we found many additional periodic orbits for our hexagonal string billiard of a different type, some of which are shown in Figs. 20 and 21.

In the captions of these figures we have used the notation $\{n_k\}$ in spite of the fact that n and k are no longer relatively prime, because we simply want to express the basic fact that the orbit has period n and that it winds around the table k times.

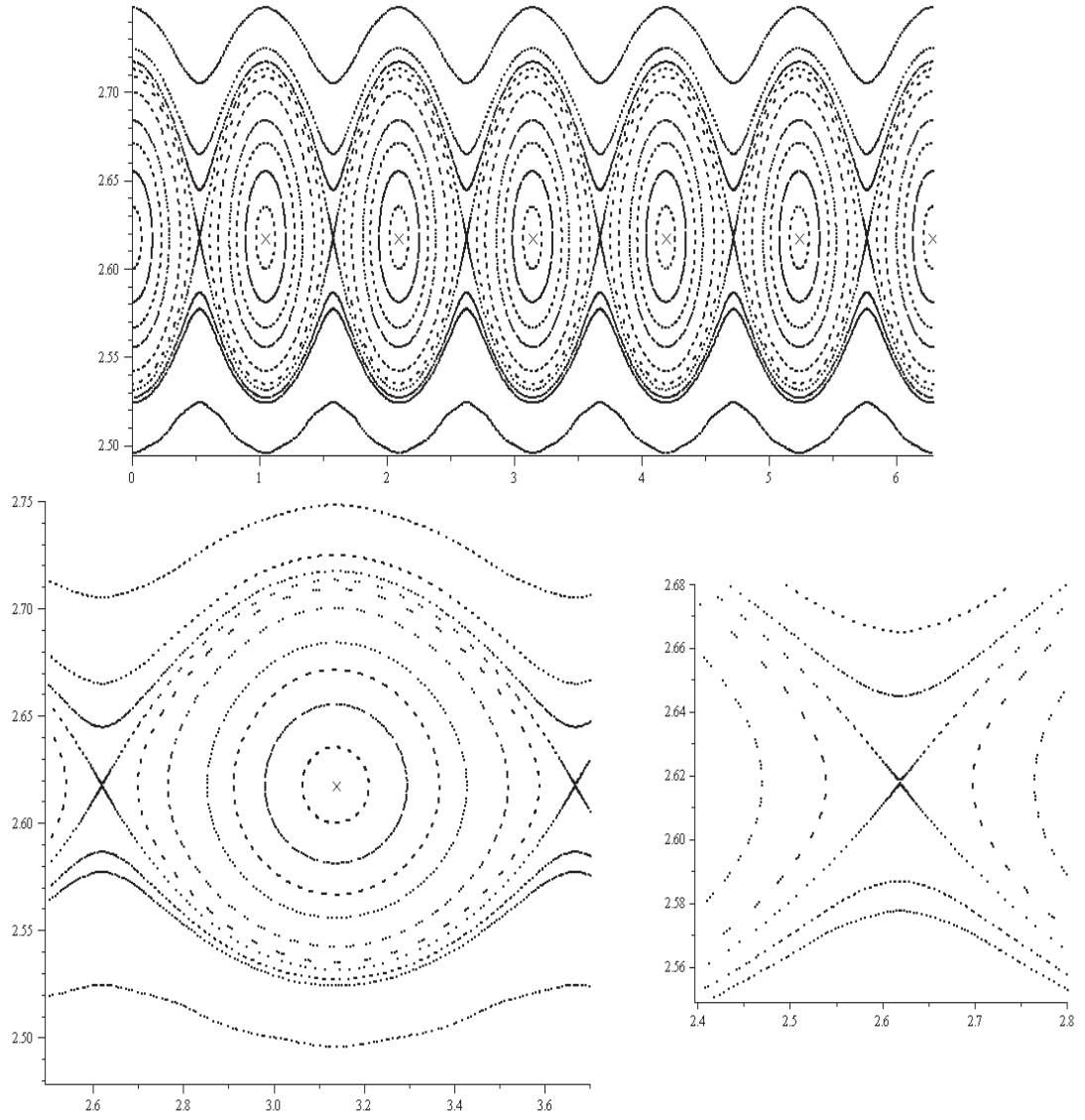


FIGURE 17. Surface of section: close-up of $\left\{\begin{smallmatrix} 6 \\ 1 \end{smallmatrix}\right\}$ orbit

Interestingly enough, all of these orbits are again isolated, but, in contrast with the ones corresponding to star polygons, these additional periodic orbits turn out to be neutrally stable!

Now let us include a brief comment about the organization of periodic and quasi-periodic trajectories in configuration space.

Periodic trajectories inside an elliptic billiard are very well organized. Recall that for fixed n and k , relatively prime positive integers with $k < n/2$, there is a continuous family of periodic orbits of the form $\left\{\begin{smallmatrix} n \\ k \end{smallmatrix}\right\}$. All the trajectories

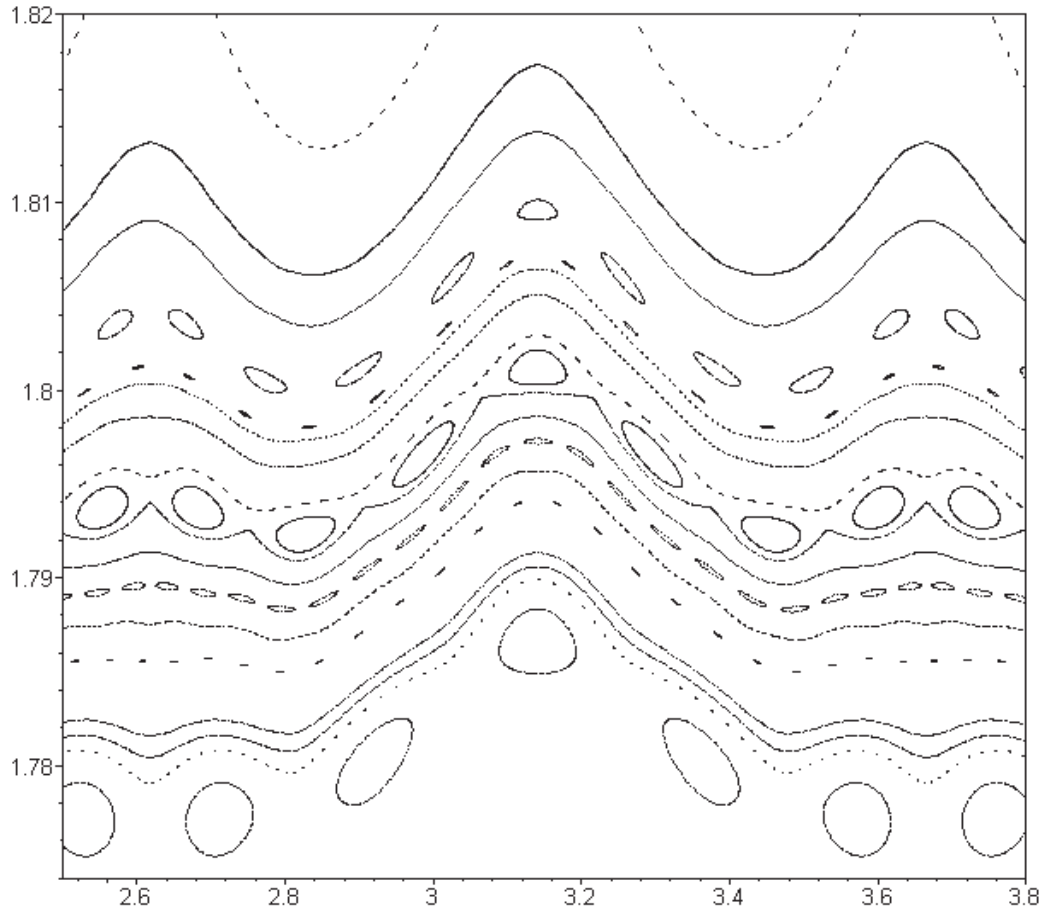


FIGURE 18. Surface of section including fat $\left\{\begin{smallmatrix} 12 \\ 5 \end{smallmatrix}\right\}$, $\left\{\begin{smallmatrix} 54 \\ 23 \end{smallmatrix}\right\}$, $\left\{\begin{smallmatrix} 7 \\ 3 \end{smallmatrix}\right\}$, and $\left\{\begin{smallmatrix} 30 \\ 13 \end{smallmatrix}\right\}$

corresponding to such a family are arranged around a common ellipse or hyperbola (see Poncelet's theorem [35]).

All periodic orbits for our billiard are isolated. So for fixed n and k , where n and k are relatively prime positive integers with $k < n/2$, we want to consider not only the periodic orbits of the form $\left\{\begin{smallmatrix} n \\ k \end{smallmatrix}\right\}$ but all the quasi-periodic orbits or fat polygons $\left\{\begin{smallmatrix} n \\ k \end{smallmatrix}\right\}$ as well. If there are any periodic orbits of the form $\left\{\begin{smallmatrix} m \\ j \end{smallmatrix}\right\}$, $j < m/2$ with $m/j = n/k$ we need to include them too. We want to see how they are organized in configuration space: if they are arranged around a common forbidden inner region.

To begin we will show what “goes on between two consecutive” unstable periodic orbits: $\left\{\begin{smallmatrix} 4 \\ 1 \end{smallmatrix}\right\}$ and $\left\{\begin{smallmatrix} 3 \\ 1 \end{smallmatrix}\right\}$.

The claim now is that for either $n = 3$ or 4 the pair of $\left\{\begin{smallmatrix} n \\ 1 \end{smallmatrix}\right\}$ unstable periodic orbits “encloses” a $\left\{\begin{smallmatrix} n \\ 1 \end{smallmatrix}\right\}$ stable periodic orbit, periodic orbits of the form $\left\{\begin{smallmatrix} m \\ j \end{smallmatrix}\right\}$, $j < m/2$ with $m/j = n$ and fat polygons $\left\{\begin{smallmatrix} n \\ 1 \end{smallmatrix}\right\}$ as well.

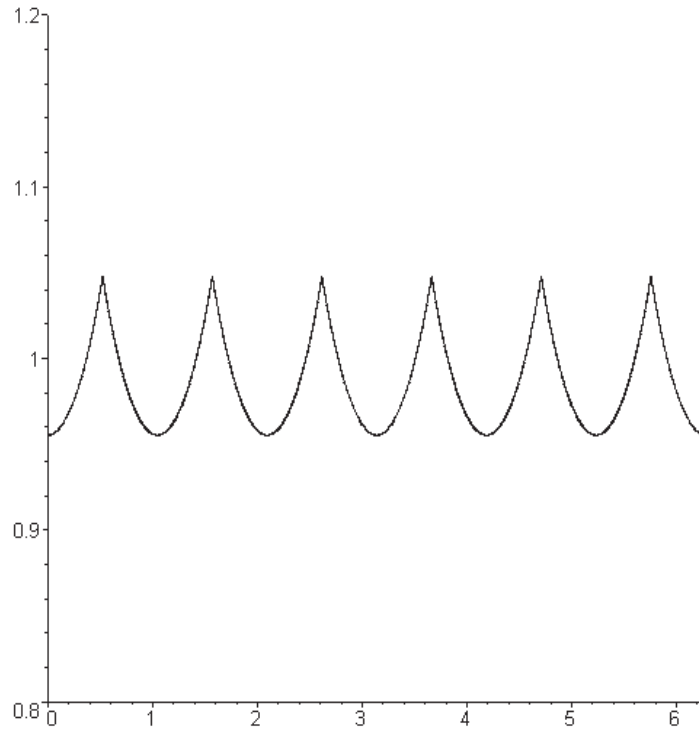


FIGURE 19. Surface of section for focal orbit

In Fig. 22 we can appreciate a pair of unstable periodic orbits $\left\{ \begin{smallmatrix} 4 \\ 1 \end{smallmatrix} \right\}$. Also included are a stable $\left\{ \begin{smallmatrix} 4 \\ 1 \end{smallmatrix} \right\}$ trajectory, a neutrally stable periodic orbit $\left\{ \begin{smallmatrix} 36 \\ 9 \end{smallmatrix} \right\}$, as well as three quasi-periodic orbits.

For the second example we start with a pair of three-bounce periodic unstable orbits. But now we have also included a Reuleaux type triangle (see Fig. 23), which will serve as a common forbidden inner region.

For the three neutrally stable periodic orbits in Fig. 24 as well as for the three quasi-periodic orbits we observe that they are confined to the region shown on the right hand side of Fig. 23.

To illustrate the general situation several pairs of consecutive unstable periodic orbits with a single quasi-periodic orbit between them are shown in Fig. 25.

To see how all the orbits related to the $\left\{ \begin{smallmatrix} 5 \\ 2 \end{smallmatrix} \right\}$ orbit are organized in configuration space see Fig. 26.

9. CONCLUDING REMARKS

EKELAND [9]: “there is no mistaking an integrable system
with a nonintegrable one.”

From the Poincaré surface of section one can get some pretty clear idea of the general behaviour a dynamical system. In it we can identify

- periodic trajectories which appear as a finite collection of points,
- quasiperiodic trajectories which appear as one-dimensional curves

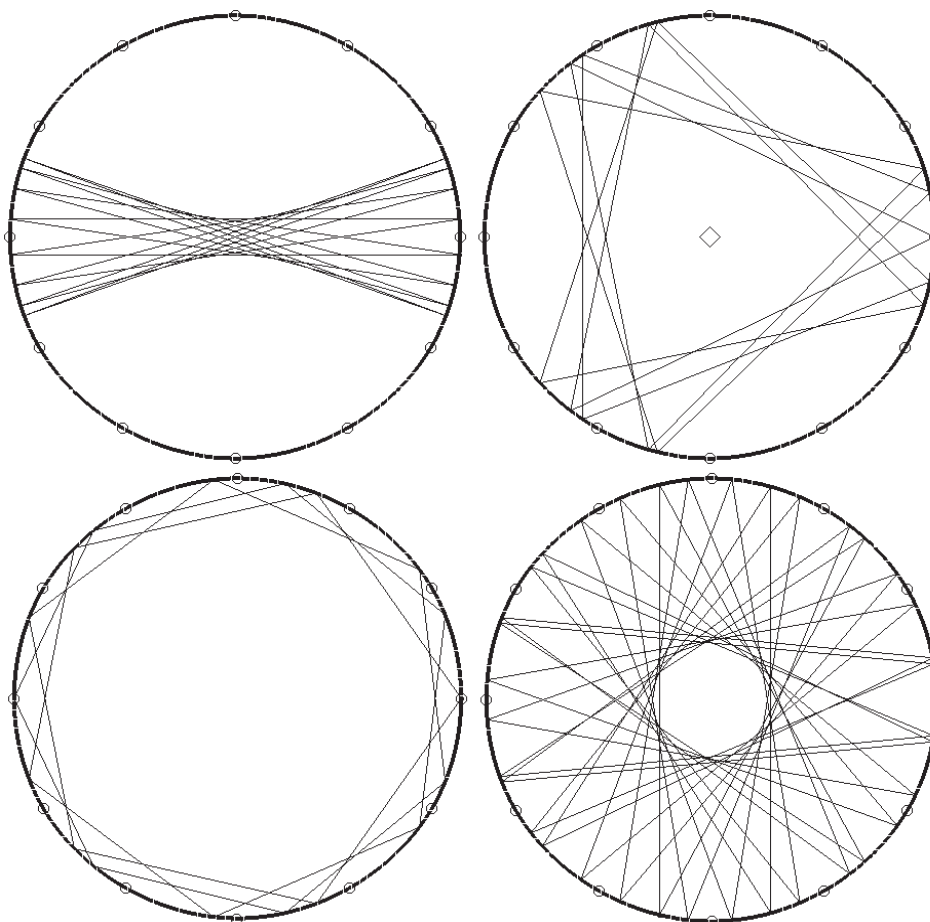


FIGURE 20. A librational, a $\left\{ \frac{15}{5} \right\}$, a $\left\{ \frac{18}{3} \right\}$, and a $\left\{ \frac{36}{15} \right\}$ orbit.

- and finally irregular or chaotic trajectories which appear as a scatter of points limited to a finite area.

In the Poincaré surface of section for a typical billiard we are able to find all of these different types of trajectories. A Poincaré surface of section consisting exclusively of closed curves and periodic points suggests completely regular (integrable) behavior.

The extreme cases of completely regular and of fully chaotic behavior are both a very uncommon occurrence. Most often one finds that the Poincaré SOS is filled with a mixture of both regular and irregular orbits (see Korsch and Zimmer [21]).

So the question is: exactly, how exceptional is the hexagonal string billiard?

The following are the most relevant properties of this billiard:

- (1) The boundary of our billiard is twice continuously differentiable and has strictly positive curvature.
- (2) Our billiard is not a simple deformation or perturbation of the circular billiard. In addition to the planar region bounded by six elliptical arcs we

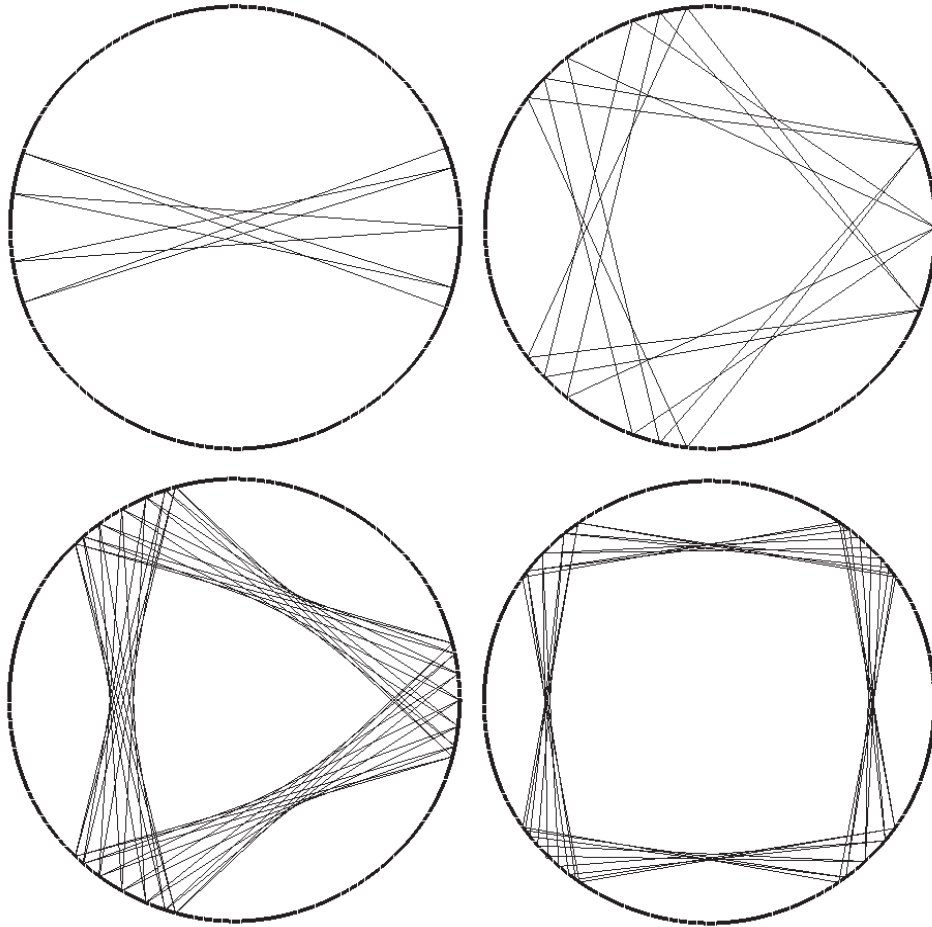


FIGURE 21. A self-retracing libration, a $\left\{ \frac{18}{6} \right\}$, a $\left\{ \frac{42}{14} \right\}$, and a $\left\{ \frac{36}{9} \right\}$ orbit.

also have a set of very special points: the foci, whose influence cannot be ignored.

- (3) Our billiard exhibits three types of trajectories: focal, outer, and inner (see Theorem 4.1).
- (4) It has a special caustic and we can associate a forbidden region with any trajectory.
- (5) The Poincaré surface of section is filled solely with periodic points and invariant curves, while chaotic area-filling orbits are totally absent.
- (6) In the Poincaré surface of section there are no island chains.

Finally let us briefly mention a long-standing open problem, very often attributed to G. D. Birkhoff, although originally stated by Poritsky [30] (see also Gutkin [15]), the so-called Birkhoff-Poritsky conjecture. It basically states that among all billiards inside smooth closed convex curves, only billiards in ellipses are integrable.

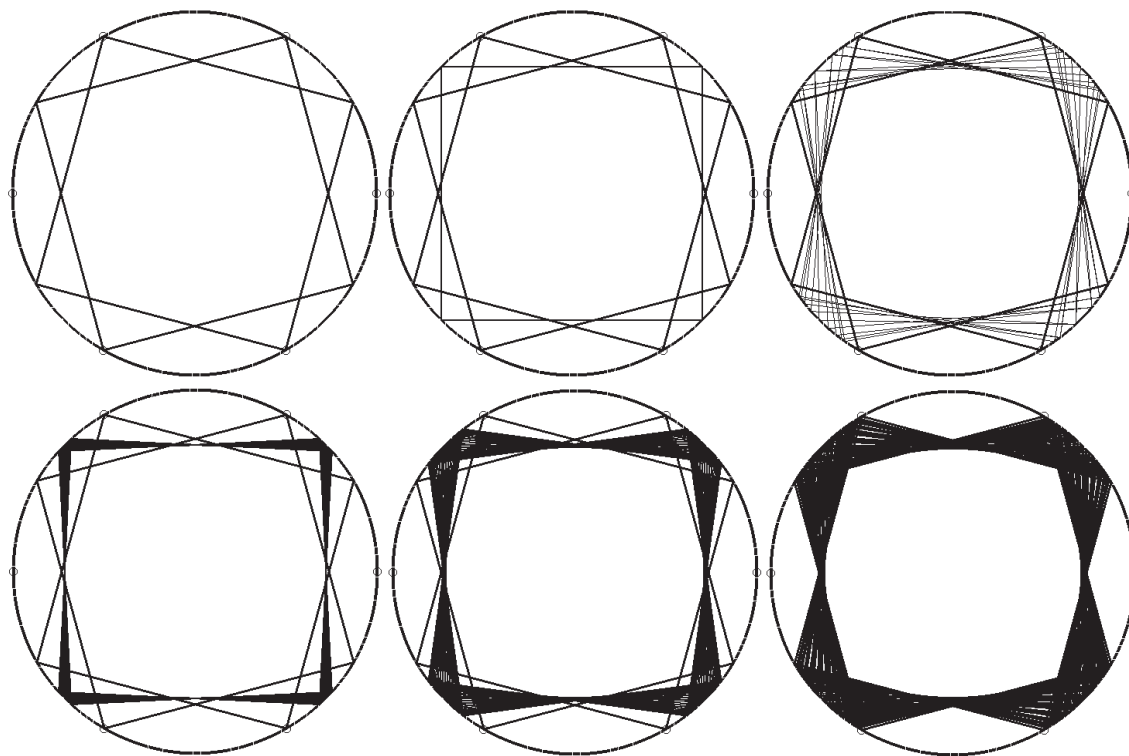


FIGURE 22. Trajectories related to the four-bounce periodic orbit

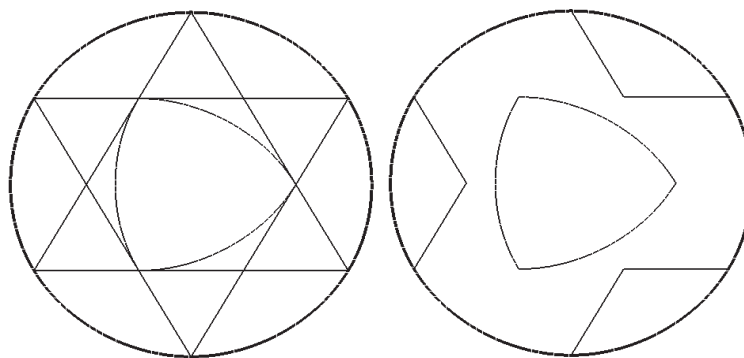


FIGURE 23. Unstable three bounce orbits and Reuleaux triangle

This means that aside from the energy, there must exist a second conserved quantity. Finding such a constant of motion is usually a very difficult task. However in the case of the elliptic billiard it is well-known: it is simply the product of the two angular momenta about the two foci (see Zhang et al. [38], Berry [4], Korsch and Zimmer [21]).

So, we want to conclude with a question:

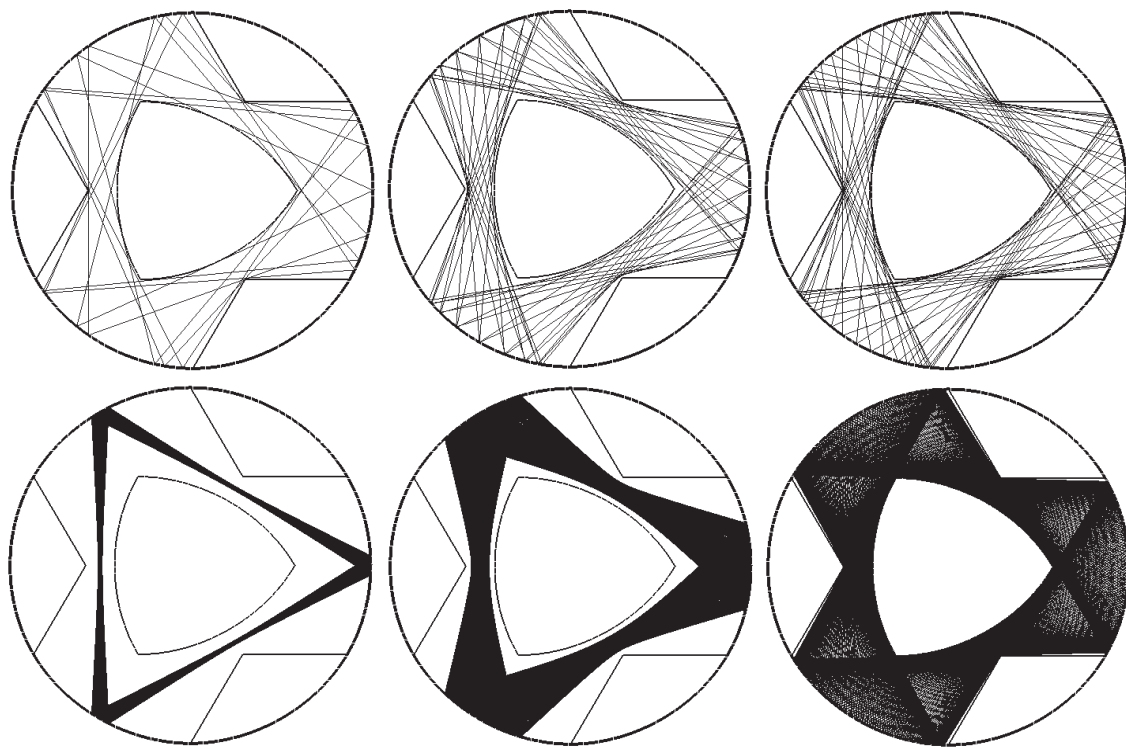


FIGURE 24. Trajectories related to the three-bounce periodic orbit

from all the evidence gathered for the hexagonal string billiard, can we still be certain that the elliptic billiard is the only integrable convex billiard?

ACKNOWLEDGEMENTS

For the extensive programming task involved in this project we have benefited greatly from Carl Eberhart's efforts, who simulates billiard-ball trajectories on both circular and elliptical tables in *Reflective paths in an ellipse*[8]. We merely have adapted some of his ideas for our own particular purposes. We also want to thank Martin Sieber for providing us, almost instantly, with a hard to get and much needed reference.

REFERENCES

- [1] P. Acquistapace, F. Broglia, Qualche calcolo sul biliardo, *Archimede* 36 (1984) 72-88.
- [2] E. Amiran, Caustics and evolutes for convex planar domains, *J. Differential Geom.* 28 (1988) 345-357.
- [3] E. Batschelet, Über einen Ausnahmefall des Wiederkehrsatzes von Poincaré, *Experientia* 4 (1948) 270.
- [4] M. V. Berry, Regularity and chaos in classical mechanics, illustrated by three deformations of a circular "billiard", *European J. Phys.* 2 (1981) 91-102.
- [5] G. D. Birkhoff, On the periodic motions of dynamical systems, *Acta Math.* 50 (1927) 359-379.
- [6] N. Chernov, R. Markarian, Chaotic billiards, in: *Mathematical Surveys and Monographs*, vol. 127, American Mathematical Society, Providence, RI, 2006.

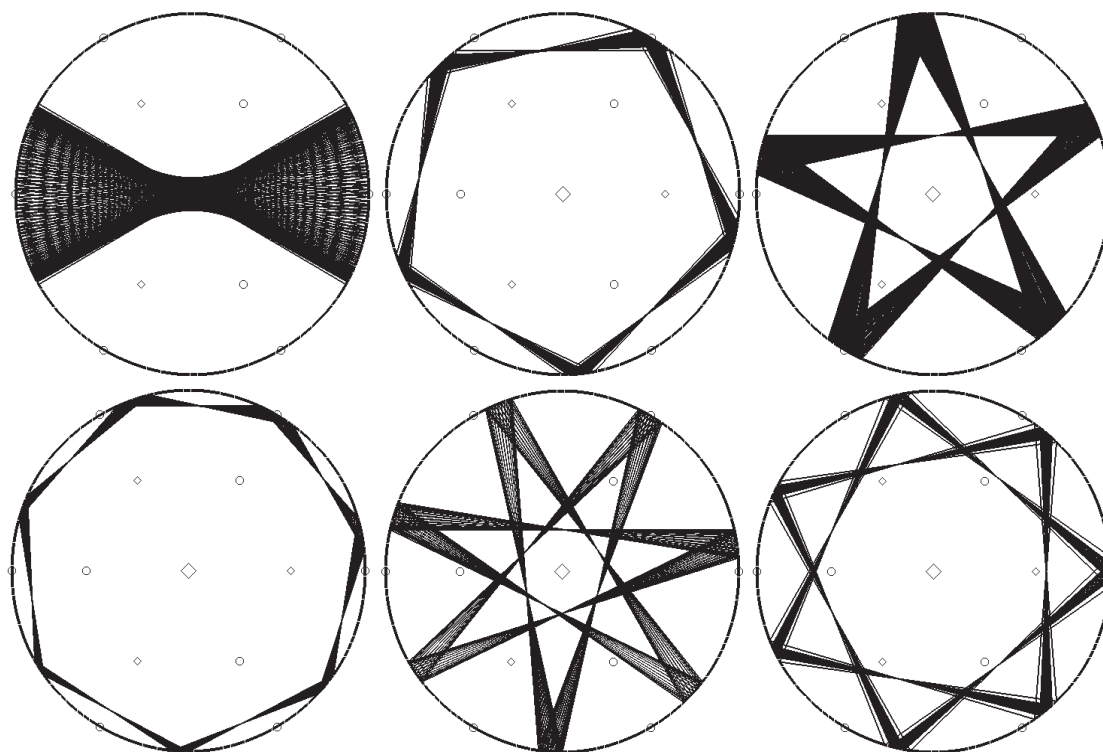


FIGURE 25. Pairs of unstable periodic orbits and single quasi-periodic orbit between them

- [7] H. T. Davis, Introduction to nonlinear differential and integral equations, Dover , New York, 1962.
- [8] C. Eberhart, Reflective paths in an ellipse, University of Kentucky, Lexington, KY
<http://www.ms.uky.edu/~car1/vps98/ellip1.html>
 last access: 28/11/2011.
- [9] I. Ekeland, The best of all possible worlds, University of Chicago Press, Chicago, 2006.
- [10] M. Frantz, A focusing property of the ellipse, Amer. Math. Monthly 101 (1994) 250-258.
- [11] S. Gardiner, Quantum Measurement, Quantum Chaos, and Bose-Einstein Condensates, PhD thesis, Leopold-Franzens-Universität Innsbruck, Austria 2000.
- [12] P. M. Gruber, Convex billiards, Geom. Dedicata 33 2 (1990) 205-226.
- [13] E. Gutkin, A. Katok, Caustics for inner and outer billiards, Comm. Math. Phys. 173 (1995) 101-133.
- [14] E. Gutkin, O. Knill, Billiards that share a triangular caustic, in: E. Lacombe, J. Llibre (Eds.) New trends in Hamiltonian systems and Celestial Mechanics, World Sci. Publ., River Edge, NJ, 1996, pp. 199-213.
- [15] E. Gutkin, Billiard dynamics: a survey with the emphasis on open problems, Regul. Chaotic Dyn. 8 (2003) 1-13.
- [16] B. Hasselblatt, A. Katok, A first course in dynamics with a panorama of recent developments, Cambridge University Press, New York, 2003.
- [17] A. Hayli, Numerical exploration of a family of strictly convex billiards with boundary of class C^2 , J. Statist. Phys. 83 (1996) 71-79.
- [18] A. Hubacher, Instability of the boundary in the billiard ball problem, Comm. Math. Phys. 108 (1987) 483-488.

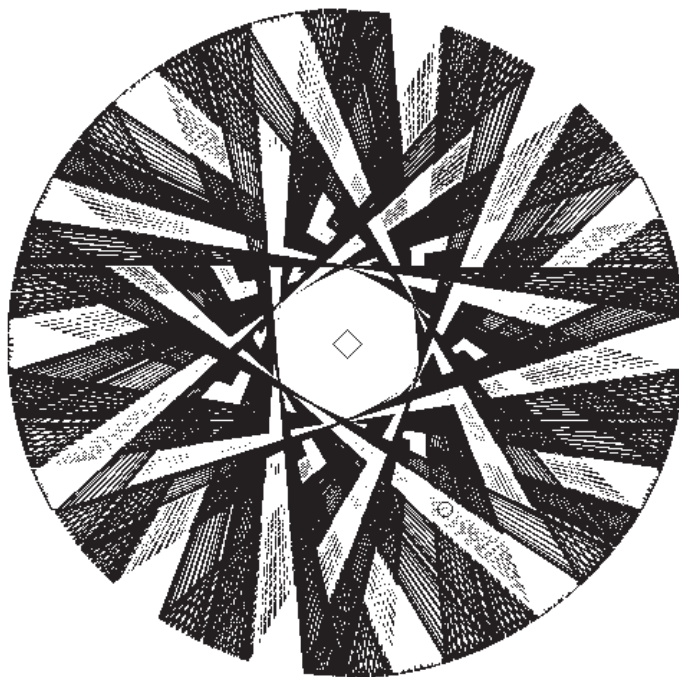


FIGURE 26. $\left\{ \begin{smallmatrix} 5 \\ 2 \end{smallmatrix} \right\}$ related orbits arranged around a common forbidden inner region

- [19] V. Klee, S. Wagon, Old and new unsolved problems in plane geometry and number theory, in: The Dolciani Mathematical Expositions, vol. 11, Mathematical Association of America, Washington, DC, 1991.
- [20] H. J. Korsch, H. -J. Jodl, Chaos: a program collection for the PC, second ed., Springer-Verlag, Berlin, 1999.
- [21] H. J. Korsch, F. Zimmer, Chaotic billiards, in: K. H. Hoffmann, M. Schreiber (Eds.), Computational statistical physics: from billiards to Monte Carlo, Springer-Verlag, Berlin, 2002, pp. 15-36.
- [22] V. Kozlov, D. Treshchëv, Billiards, Translations of Mathematical Monographs, American Mathematical Society, vol. 89 Providence, RI, 1991.
- [23] V. Lazutkin, Existence of caustics for the billiard problem in a convex domain, *Izv. Akad. Nauk SSSR Ser. Mat.* 37 (1973) 186-216.
- [24] V. Lopac, I. Mrkonjić, D. Radić, Chaotic behavior in lemon-shaped billiards with elliptical and hyperbolic boundary arcs, *Physical Review E - Statistical, Nonlinear, and Soft Matter Physics* 64 (2001) 016214/1-016214/8.
- [25] V. Lopac, I. Mrkonjić, N. Pavin, D. Radić, Chaotic dynamics of the elliptical stadium billiard in the full parameter space, *Phys. D* 217 (2006) 88-101.
- [26] J. Mather, Glancing billiards, *Ergodic Theory Dynam. Systems* 2 (1982) 397-403.
- [27] J. Moser, E. J. Zehnder, Notes on dynamical systems, Courant Lecture Notes in Mathematics, New York University, New York, vol. 12, 2005.
- [28] S. Okai, H. Nishioka, M. Ohta, Periodic orbits in elliptic billiards, *Mem. Konan Univ. Sci. Ser.* 37 (1990) 29-45.
- [29] K. Poorrezaei, Two proofs of Graves's theorem, *Amer. Math. Monthly* 110 (2003) 826-830.
- [30] H. Poritsky, The billiard ball problem on a table with a convex boundary—an illustrative dynamical problem, *Ann. of Math. (2)* 51 (1950) 446-470.

- [31] M. Robnik, Classical dynamics of a family of billiards with analytic boundaries, *J. Phys. A* 16 (1983) 3971-3986.
- [32] K. Siburg, The principle of least action in geometry and dynamics, *Lecture Notes in Mathematics*, vol. 1844, Springer-Verlag, Berlin, 2004.
- [33] M. Sieber, Semiclassical transition from an elliptical to an oval billiard, *Journal of Physics A* 30 (1997) 4563-4596.
- [34] G. J. Sussman, J. Wisdom, M. E. Mayer, *Structure and interpretation of classical mechanics*, MIT Press, Cambridge, 2001.
- [35] S. Tabachnikov, *Billiards*, Panoramas et Synthèses, Société Mathématique de France, vol. 1, 1995.
- [36] P. H. Turner, Convex caustics for billiards in \mathbb{R}^2 and \mathbb{R}^3 , in: D. C. Kay, M. Breen (Eds.), *Convexity and Related Combinatorial Geometry*, Dekker, New York, 1982, pp. 85-106.
- [37] J. B. Wilker, Further thoughts on a focusing property of the ellipse, *Bull. Belg. Math. Soc. Simon Stevin* 2 2 (1995) 153-159.
- [38] J. Zhang, A. Merchant, W. Rae, Geometric derivations of the second constant of motion for an elliptic "billiard" and other results, *European J. Phys.* 15 (1994) 133-138.

APPENDIX A.

Proof of Theorem 2.1. Consider now the ellipses \mathcal{E}_1 with foci F_1, F_3 and \mathcal{E}_n with F_n, F_2 and where the sum of the distances from the two foci is given by $l - 2(n-2) = 2 + 2d$. The length of the portion of the string that is in contact with the n -gon is $2(n-2)$.

The ellipses \mathcal{E}_1 and \mathcal{E}_n are of course very smooth closed curves and we need merely verify that the equation for \mathcal{E}_1 has the same function value and first and second derivatives as the equation for \mathcal{E}_n at $x = 0$ thus ensuring C^2 continuity (see Fig. 2).

Letting $P(x, y)$ be an arbitrary point, then for the ellipse \mathcal{E}_1 :

$$|F_1P| + |F_3P| = 2 - \frac{2}{\cos \alpha}$$

or

$$\sqrt{(x+1)^2 + y^2} + \sqrt{(x-1+2\cos\alpha)^2 + (y+2\sin\alpha)^2} = 2 - \frac{2}{\cos\alpha}$$

Similarly, for the ellipse \mathcal{E}_n :

$$|F_nP| + |F_2P| = 2 - \frac{2}{\cos \alpha}$$

or

$$\sqrt{(x+1-2\cos\alpha)^2 + (y+2\sin\alpha)^2} + \sqrt{(x-1)^2 + y^2} = 2 - \frac{2}{\cos\alpha}$$

By bringing all the terms from the right-hand side to the left-hand side, we get the equations

$$e_1(x, y) = 0 \quad \text{and} \quad e_n(x, y) = 0$$

Notice that since

$$e_n(x, y) = e_1(-x, y)$$

the values of the functions and of the second derivatives for the equations of both ellipses have to coincide when $x = 0$.

A simple, but tedious process of straightforward differentiation and substitution shows that at the common intersection point $G_1 = (0, -\frac{\sin\alpha}{\cos\alpha})$ the first derivative is 0 and the second derivative is $(\cos\alpha - 1) \cos\alpha \sin\alpha / (-1 + 2\cos\alpha)$ for both equations.

□

APPENDIX B.

Proof of Theorem 4.1.

- i) There are two extreme supporting lines at each vertex and any ray that lies in the angle formed by the them is also a supporting line of K .

So to start, without loss of generality, let us consider a billiard segment that lies in the angle formed by the two extreme supporting lines at vertex F_2 . It will have necessarily one extreme point on arc $\widehat{24}$ and the other on arc $\widehat{62}$. If the extreme point on arc $\widehat{24}$ is chosen as the initial point P_0 then we get a ray passing through the vertex F_2 which will then intersect the arc $\widehat{62}$ at some point P_1 .

Because of the reflective property of ellipses a ray leaving one focus, in this case F_2 , will reflect off the ellipse corresponding to the arc $\widehat{62}$ and pass through the second focus F_6 .

But then we get again a ray (through P_1 and F_6) that lies in the angle formed by the two extreme supporting lines for the vertex F_6 so it has to be on a supporting line itself.

That just means that the billiard trajectory remains on a supporting line.

- ii) Let us now consider the angle formed by the two supporting lines of K through a point P_0 on arc $\widehat{24}$. One of them goes through F_2 and the other through F_4 . Because of this they are also supporting lines of the closed segment F_2F_4 , which is the segment between the two foci of the ellipse corresponding to arc $\widehat{24}$. Now we can consider two different types of rays issuing from P_0 : those strictly inside and those strictly outside the convex angle $F_2P_0F_4$. The first ones will intersect the interiors of both K and of the segment F_2F_4 (see[29]), whereas the second ones do not intersect either K or the closed segment F_2F_4 .

In the first case we get a segment P_0P_1 where P_1 is some point belonging to the arc $\widehat{j, j+2}$. Let us consider the reverse trajectory, the one starting at point P_1 and ending at point P_0 . It, of course, intersects the interior of K . But then it has to intersect the interior of the segment F_jF_{j+2} . So then the original trajectory intersects this segment and it has to do so again after reflection with the boundary. This implies that the reflected segment of the trajectory then also intersects the interior of K .

- iii) We leave this case to the reader.

□

APPENDIX C.

Proof of Theorem 4.2. Because of the symmetry present in our billiard, we can restrict attention to a typical arc, say $\widehat{24}$.

Let $P(x, y)$ be a point on this arc (See Fig. 3). Then

$$\cos \gamma = \frac{-12 + a^2 + b^2}{2ab},$$

where

$$a = \sqrt{(x-1)^2 + (y + \sqrt{3})^2}, b = \sqrt{(x-1)^2 + (y - \sqrt{3})^2}$$

so

$$\cos \gamma = \frac{-12 + 2(x-1)^2 + (y + \sqrt{3})^2 + (y - \sqrt{3})^2}{2\sqrt{(x-1)^2 + (y + \sqrt{3})^2}\sqrt{(x-1)^2 + (y - \sqrt{3})^2}}$$

Substituting the equation for the ellipse

$$(x-1)^2 = 6\left(1 - \frac{y^2}{9}\right)$$

we get

$$\cos \gamma = \frac{\frac{-4y^2}{3} + (y + \sqrt{3})^2 + (y - \sqrt{3})^2}{2\sqrt{6 - \frac{2y^2}{3} + (y + \sqrt{3})^2}\sqrt{6 - \frac{2y^2}{3} + (y - \sqrt{3})^2}}$$

or after simplifying

$$\cos \gamma = \frac{y^2 + 9}{27 - y^2}$$

Since

$$-\sqrt{3} \leq y \leq \sqrt{3}$$

it is easy to see that

$$\frac{1}{3} \leq \cos \gamma \leq \frac{1}{2}$$

so that

$$60^\circ \leq \gamma \leq 70.53^\circ$$

□

APPENDIX D.

Proof of Theorem 4.3. For the notation see Fig. 9. Consider the sequences $\{s_i\}, \{\varphi_i\}, \{\alpha_i\}$. It is clear that they are bounded:

- $2 \leq s_i \leq 4$
- $\pi/6 \leq \varphi_i \leq \pi/2$
- $\pi/3 \leq \alpha_i \leq \arccos(\frac{1}{3})$ (see Thm.4.2).

We will show that $\{\varphi_i\}, \{s_i\}$ are both nondecreasing sequences.

Subtracting

$$\varphi_{i+1} + \varphi'_{i+1} = 2\pi/3$$

from

$$\alpha_i + \varphi_i + \varphi'_{i+1} = \pi$$

we get

$$0 \leq \alpha_i - \pi/3 = \varphi_{i+1} - \varphi_i$$

and therefore $\varphi_i \leq \varphi_{i+1}$.

From

$$s_i^2 = 12 + t_i^2 - 2 \cdot 2\sqrt{3}t_i \cos \varphi_i$$

and

$$s_i + t_i = 6$$

we get

$$s_i = \frac{4\sqrt{3} - 6 \cos \varphi_i}{\sqrt{3} - \cos \varphi_i}$$

Note that the function $f(\varphi) = \frac{4\sqrt{3}-6\cos\varphi}{\sqrt{3-\cos\varphi}}$ is nondecreasing.

So if $\varphi_i \leq \varphi_{i+1}$ then $s_i = f(\varphi_i) \leq f(\varphi_{i+1}) = s_{i+1}$.

Now $\{\varphi_i\}$ and $\{s_i\}$ both converge because they are monotone bounded sequences.

But then as $i \rightarrow \infty$

$$\alpha_i - \pi/3 = \varphi_{i+1} - \varphi_i \rightarrow 0$$

and therefore

$$\alpha_i \rightarrow \pi/3$$

From

$$12 = s_i^2 + t_i^2 - 2s_it_i \cos \alpha_i$$

and

$$s_i + t_i = 6$$

we obtain

$$\cos \alpha_i = -\frac{12 + s_i^2 - 6s_i}{s_i(-6 + s_i)}$$

So if $i \rightarrow \infty$ then $s_i \rightarrow s^*$ and

$$\frac{1}{2} = -\frac{12 + s^{*2} - 6s^*}{s^*(-6 + s^*)}$$

which yields $s^* = 2, 4$.

Using the law of sines we get

$$\frac{\sin \alpha_i}{\sqrt{12}} = \frac{\sin \varphi_i}{s_i}$$

if $i \rightarrow \infty$ then

$$\frac{\sqrt{3}/2}{\sqrt{12}} = \frac{\sin \varphi^*}{4}$$

that is

$$\sin \varphi^* = 1$$

and so finally

$$\varphi^* = \frac{\pi}{2}$$

□